HITTITE JOURNAL OF SCIENCE AND ENGINEERING

e-ISSN: 2148-4171
Volume: 12 • Number: 1
March 2025

Effect of Double-Pulse Strategy on the Expulsion Formation and Peak Loads During Resistance Spot Welding of Dissimilar Thickness Ultra - High Strength MS1500 and Mild DD11 Steels

Mehmet Okan Görtan
Hacettepe University, Department of Mechanical Engineering, Ankara, Türkiye.

Corresponding Author
Mehmet Okan Görtan
E-mail: okangortan@hacettepe.edu.tr Phone: +90 312 297 62 08 Fax: +90 312 297 62 06
RORID: https://ror.org/04kwvgz42

Article Information
Article Type: Research Article
Doi: https://doi.org/10.17350/HJSE19030000351
Received: 21.01.2025
Accepted: 21.03.2025
Published: 25.03.2025

Cite As
Görtan MO. Effect of Double-Pulse Strategy on the Expulsion Formation and Peak Loads During Resistance Spot Welding of Dissimilar Thickness Ultra - High Strength MS1500 and Mild DD11 Steels. Hittite J Sci Eng. 2025;12(1):51-58.

Peer Review: Evaluated by independent reviewers working in at least two different institutions appointed by the field editor.
Ethical Statement: Not available.
Plagiarism Checks: Yes - iThenticate
Conflict of Interest: Authors declare no conflict of interest.

CRediT AUTHOR STATEMENT
Mehmet Okan Görtan: Funding acquisition, Conceptualization, Methodology, Investigation, Data curation, Visualization, Validation, Writing- original draft.

Effect of Double-Pulse Strategy on the Expulsion Formation and Peak Loads During Resistance Spot Welding of Dissimilar Thickness Ultra - High Strength MS1500 and Mild DD11 Steels

Mehmet Okan Görtan

Hacettepe University, Department of Mechanical Engineering, Ankara, Türkiye.

Abstract

Resistance spot welding (RSW) is widely utilized in the automotive industry due to its high efficiency, flexibility, and compatibility with automation. These advantages make it a preferred method for joining advanced high-strength steels, enabling lightweight designs without compromising structural integrity. This study explores the mechanical properties of resistance spot-welded joints between ultra-high-strength MS1500 steel and hot-rolled DD11 steel, with a focus on single-pulse and double-pulse welding strategies. The effects of varying current levels were evaluated in terms of tensile-shear strength, failure energy, nugget diameter, hardness distribution, and microstructural transformations. In single-pulse welding, expulsion was observed at a current of 8.6 kA, limiting joint performance. Conversely, the double-pulse welding strategy provided enhanced control, yielding superior results. Optimal performance was achieved at a second welding current of 8.4 kA, with a tensile-shear strength increase of 11.6% and a fracture energy enhancement of 32.2% compared to single-pulse welding. Beyond 8.6 kA, expulsion caused inconsistencies in mechanical properties, highlighting the importance of current optimization in welding strategies. The findings demonstrate the effectiveness of the double-pulse welding strategy in improving the strength and quality of resistance spot-welded joints.

Keywords: Resistance spot welding, Ultra-high strength steel, Double-pulse welding, Expulsion, Mechanical strength

INTRODUCTION

One of the most significant trends that has marked the automotive industry over the last 20 years is weight reduction. The most commonly employed strategy to achieve this is replacing the materials used with higher-strength alternatives. This approach enables the reduction of vehicle weight by carrying the same loads with smaller cross-sections without compromising passenger safety [1]. Due to its flexibility in application, high efficiency, and suitability for automation, resistance spot welding (RSW) has become the preferred method for joining high-strength sheets, particularly in the automotive industry [2]. Therefore, improving the mechanical strength of RSW joints holds great importance.

An electric current is passed through sheet materials, typically held together by pressurized electrodes that are actively cooled during RSW. The heat energy generated by the flow of electricity causes a rapid temperature increase in a relatively small area between the sheets, allowing the molten metals to bond within a short time [3]. In the RSW process, the rapid cooling of the molten metal in the nugget region after welding enables the formation of martensitic microstructures with high mechanical strength in steel sheets [4]. Therefore, RSW is currently widely used, especially in the automotive industry, for joining advanced high-strength steel sheets [5-7].

The most common traditional method to improve the mechanical properties of RSW joints is to optimize the welding current and duration. The main determining factor here is to maximize the nugget diameter in the joint area without causing expulsion [8]. In recent years, a technology frequently referred to as double-pulse welding has been employed. In this method, the welding current is interrupted in the first step before expulsion occurs, followed by the application of a higher or lower current in a second welding step [9-13]. This approach allows for increasing the nugget diameter without expulsion, which negatively affects joint stability, thereby enhancing mechanical strength.

In addition, the use of metals with different strength and metallurgical properties together is a common practice, especially in the automotive industry. RSW can also be used to join these materials. In the current studies, it is shown that RSW can also be used to join advanced high-strength steel sheets of different types and thicknesses based on specific application needs [14-19].

In the current study, the RSW properties of ultra-high-strength MS1500 steel and hot-rolled DD11 (1.0332) steel of varying thicknesses were investigated. Those kind of joints are required recently especially in the bumper beam sections of passenger vehicles. In preliminary studies, expulsion limit of the joint in single-pulse strategy was determined. Afterwards, the effects of the double-pulse welding strategy using different current values were investigated. Mechanical strength of the joints was determined using tensile-shear tests. After the mechanical testing of the joints, the types of fractures that occurred were examined using optical microscopy. The strength and the various fracture modes observed were discussed along with the microstructural properties.

MATERIAL AND METHODS

In the experimental studies, martensitic micro-structured ultra-high-strength MS1500 steel with a thickness of 1.2 mm and hot-rolled DD11 drawing steel with a thickness of 2.0 mm were used. The chemical compositions of these materials are shown in Table 1. The MS1500 steel contains 0.271% carbon and 0.770% manganese. On the other hand, the DD11 steel has very low carbon content but relatively high manganese content of approximately 0.219%. Accordingly, a martensitic transformation in the microstructure can be expected in both materials after rapid cooling from the austenitic region.

Table 1. Alloy composition of the investigated materials (weight %).

Material	C	Si	Mn	Al	Ti	Cr	B	Cu	Fe
DD11	0.057	-	0.219	0.045	-	-	-	-	balance
MS1500	0.271	0.207	0.770	0.268	0.036	0.023	0.010	0.116	balance

The mechanical properties of the material were determined using specimens with a nominal width of 12.5 mm and a nominal gauge length of 50 mm in accordance with the ISO 6892-1:2009 standard. For this purpose, five tests were conducted, and the average results of these tests are presented in Table 2.

Table 2. Mechanical properties of the investigated materials.

Material	Yield Strength [MPa]	Tensile Strength [MPa]	Alongation at Fracture [%]
DD11	272.3	372.3	34.5
MS1500	1459.2	1643.8	5.5

The specimens to be used in RSW trials were mechanically cut to dimensions of 105 x 45 mm in accordance with the ISO 14273:2016 standard. These specimens were positioned and joined as shown in Figure 1, in compliance with the standard. DD11 samples are put on top and MS1500 samples are at the bottom during welding. That way, welding of dissimilar materials is realized. After the welding process, support plates were welded to prevent additional deformation in the nugget region during the tensile-shear test. The arrows in the figure indicate the pulling directions during the tensile-shear test.

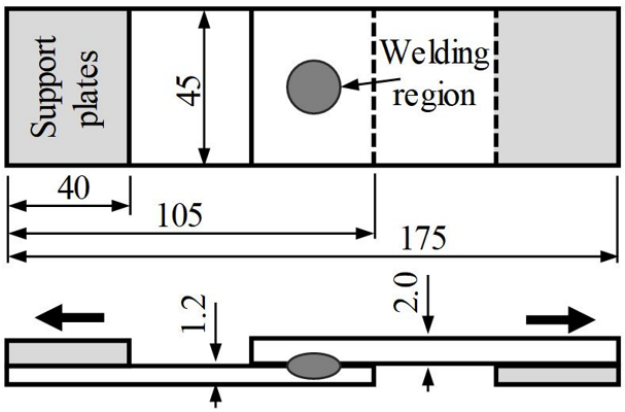

Figure 1: Geometry of the resistance spot welded specimens (All dimensions in mm).

All welding operations were performed using a 70 kVA capacity, water-cooled, pneumatically operated pedestal-type RSW machine with numerically controlled welding current, duration, and electrode pressure. This machine operates at 50 Hz frequency, identical to the electrical grid, meaning one welding cycle lasts 20 milliseconds. The primary welding parameters in this study were determined in accordance with the recommendations of the American Welding Society.

First, since sheets of different thicknesses were used, the equivalent sheet thickness was calculated using the formula provided in Eq. 1:

$$t_{eq} = t_{thin} + \left[0.2 * \left(t_{thick} - t_{thin}\right)\right] \quad (1)$$

Here t_{eq} represents the equivalent thickness, t_{thin} is the thickness of the thinner sheet, and t_{thick} is the thickness of the thicker sheet.

Based on the calculated equivalent thickness value of 1.36 mm, electrodes compliant with ISO 5821:2009 standards, type G0 with an 8 mm contact diameter and a height of 20 mm, were used in the welding process. These electrodes were manufactured from type A 2/3 copper alloyed with chromium and zirconium, as specified by ISO 5182:1991.

The electrode force applied in the study was set to 3.5 kN. The welding duration for each operation was set to 12 cycles, equivalent to 0.24 seconds. The hold time after welding was chosen as 20 cycles, or 0.40 seconds.

During single-pulse welding, expulsion was observed at current values above 8.6 kA. Therefore, 8.6 kA was chosen as the starting value for this study. In double-pulse welding, after applying an 8.6 kA current for 12 cycles, a 2-cycle (0.04-second) pause was introduced. Subsequently, in the second stage, currents ranging between 7.2 and 9.6 kA, increasing incrementally by 0.2 kA, were applied for another 12 cycles.

In both welding strategies, the squeeze time before welding was set to 50 cycles. Similarly, the electrode release time after the completion of each welding operation was also set to 50 cycles. The applied welding strategy is schematically illustrated in Fig. 2.

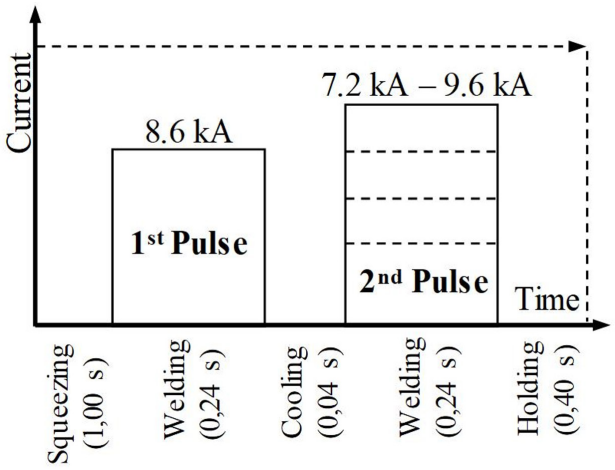

Figure 2: Schematic view of the pulse scheme.

For each welding current value planned for investigation in the study, 10 specimens were produced. To ensure the statistical significance of the tensile-shear test results, 9 of these specimens were used for testing. All tests were conducted in accordance with the ISO 14273:2016 standard using a servo-mechanical UTEST universal tensile testing machine with a 50 kN capacity at a constant speed of 10 mm/min.

The tensile-shear strength and fracture energy of the joints were determined from the force-displacement curves of the applied tests. These results are shown as an example in Fig. 3. The highest value on the force-displacement curve is considered the tensile-shear strength of the joint.

The fracture energy is defined as the area under the force-displacement curve up to the maximum load value and is calculated using Eq. 2:

$$FE = \sum_{n=1}^{n_{max}} F(n) * \left[x(n) - x(n-1)\right] \quad (2)$$

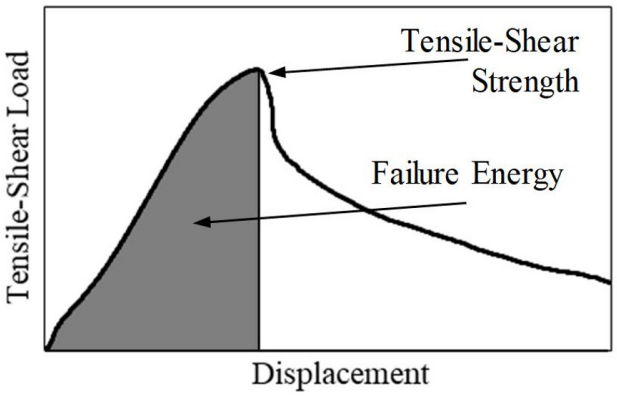

Figure 3: Schematic representation of load-displacement curve results.

Here F is the load in Newtons, x is the displacement in millimeters, n is the total number of data points, and n_{max} is the number of data points corresponding to the maximum force measured.

One of the welded specimens was used for geometry and microstructure analyses. For this purpose, the specimens were abrasively cut at their central regions and mounted in cold bakelite. Subsequently, they were ground with papers ranging from P400 to P2500 grit and polished using a 1µm diamond suspension. To examine the microstructure and perform geometric measurements, the specimens were etched with 4% Nital solution for approximately 10 seconds. Optical measurements were carried out using an Optika IM-3MET microscope. In this study, specific measurements of the nugget diameter and indentation geometry were conducted. The indentation value was determined using Eq. 3:

$$indentation = t_{thin} + t_{thick} - weld\ \ height \quad (3)$$

Here t_{thin} is the thickness of the thinner sheet, t_{thick} is the thickness of the thicker sheet, and *weld height* is the measured joint section thickness. These dimensions are schematically illustrated in Fig. 4.

Microstructure analyses were performed using a Hitachi SU5000 scanning electron microscope. The hardness measurements of the specimens were conducted in accordance with the ISO 6507-1:2018 standard using a Future Tech FM-700e device with a 100 g load and a dwell time of 15 seconds. All measurements were taken along a section starting in the base metal of DD11 material, going through the nugget, and ending in the base metal of MS1500 steel.

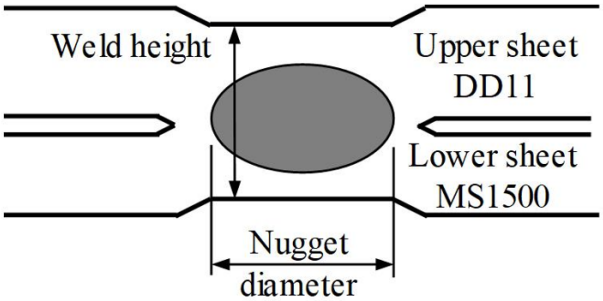

Figure 4: Schematic representation of joint section.

RESULTS AND DISCUSSION

The tensile-shear test results of the specimens produced using different current values and welding strategies are shown in Fig. 5. In this figure, the average results of the 9 tests performed are presented along with the standard deviation of the results. At the current value of 8.6 kA, which is the limit for the single-pulse welding application, the tensile-shear force and fracture energy values were determined as 18.32 kN and 33.27 J, respectively. Additionally, in this case, the standard deviation values for the tensile-shear force and fracture energy were calculated as 0.84 kN and 1.90 J, respectively.

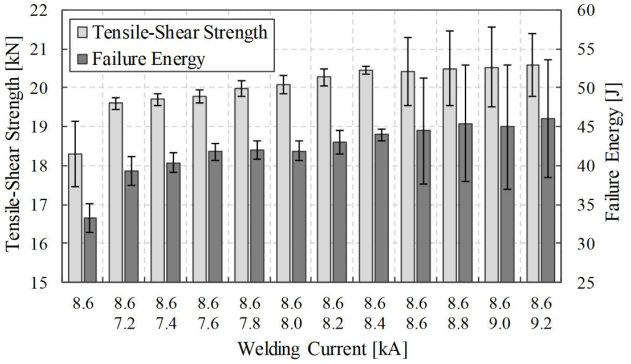

Figure 5: Tensile-shear test results of trials with different current values.

When the double-pulse welding strategy was applied, a consistent increase in strength values and a regular decrease in standard deviation values were noted until the second welding current reached 8.4 kA. However, when the second welding current increased to 8.6 kA, the increase in mechanical strength values ceased, and a significant rise in standard deviation values was observed. As a result, for the condition where the first and second pulse welding currents were 8.6 kA and 8.4 kA, respectively, which yielded the highest mechanical strength, the tensile-shear strength and fracture energy were determined as 20.45 kN and 43.98 J, respectively. In this condition, compared to the single-pulse welding application, an increase of 11.6% in tensile-shear strength and 32.2% in fracture energy was observed. Furthermore, in the double-pulse welding application with the highest strength, the standard deviation values were determined as 0.09 kN for tensile-shear strength and 0.79 J for fracture energy. However, no improvement in mechanical strength was observed when the second current value was

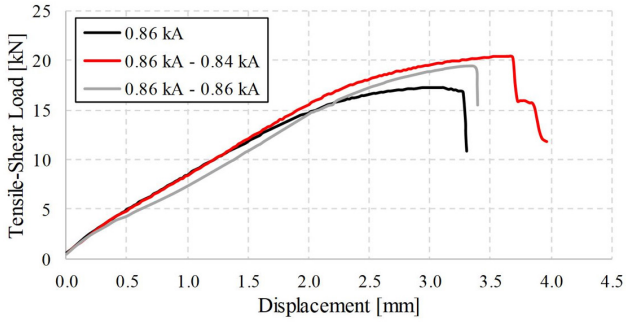

Figure 6: Example of tensile-shear test results.

8.6 kA or higher. On the contrary, the standard deviation values of the measurements increased significantly.

The differences can be better understood by analyzing the tensile-shear test results in detail. Fig. 6 shows sample test results for three different cases. When single-pulse welding is applied, relatively low strength and low deformation before fracture are observed. Accordingly, the results shown in Fig. 5 are obtained. For the case where the highest strength is achieved using the double-pulse welding strategy, the deformation at the moment of fracture is greater compared to other cases. Additionally, it is observed that the test specimens do not break suddenly; after reaching the maximum strength, the sheets separate from each other only after undergoing additional deformation. Consequently, the failure energy values are also higher compared to other cases. However, when the current value in the double-pulse welding strategy exceeds 8.6 kA, the maximum strength values decrease, and the specimens fracture suddenly. Lastly, a common feature of all tensile-shear tests is that the force increases rapidly at the beginning but slows down as it approaches fracture. This has been interpreted as an indication that the lower-strength DD11 steel undergoes additional deformation before fracture.

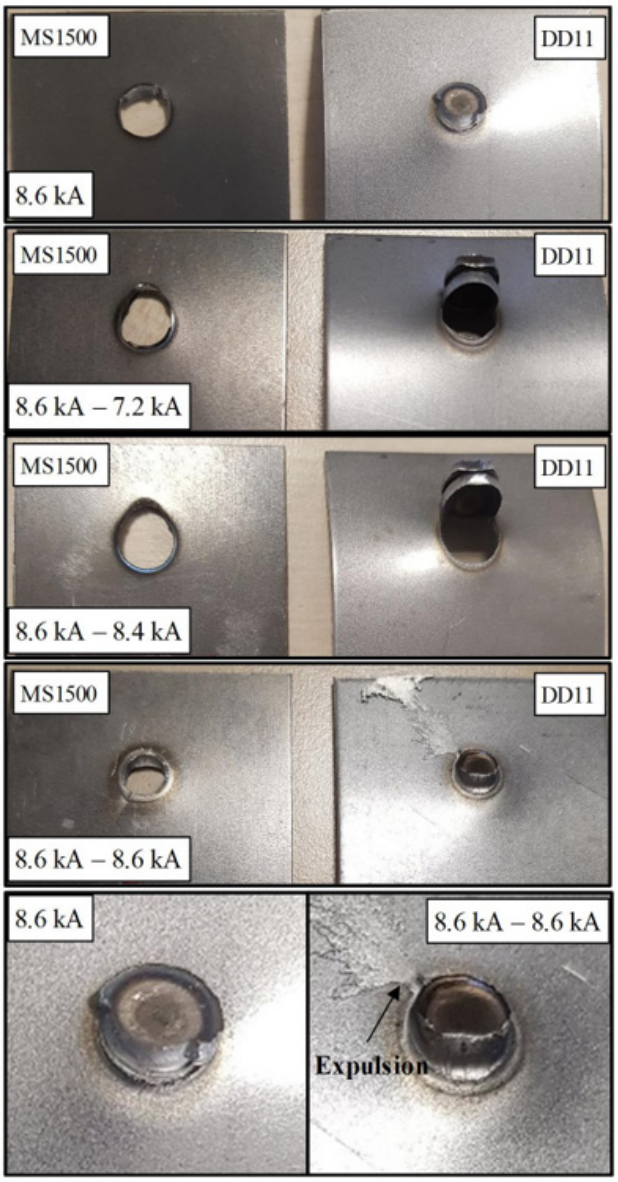

Figure 6: Fracture pictures of the joints generated using different currents (Detail views of fracture is given in the bottom pictures).

This situation observed in the results can be explained by the fracture images of the weld region shown in Fig. 7, the nugget diameter distribution in Fig. 9, the changes in indentation depth shown in Fig. 10, and the force-displacement diagrams provided as an example in Figure 11. In Fig. 7, it is shown that when a single-pulse welding current of 8.6 kA is applied, the weld region fractures in the form of partial pull-out and partial interfacial failure, and no expulsion occurs during welding. When double-pulse welding is applied, even at the lowest second current value of 7.2 kA examined, the fracture occurs in the form of full pull-out failure. A similar observation is valid for the current value at which the highest strength is achieved. However, when the double-pulse welding current is increased to 8.6 kA, expulsion occurs in the weld region, and the fracture happens as partial pull-out and partial interfacial failure. In the RSW process, expulsion occurs randomly and cannot be controlled. Consequently, differences in mechanical strength values arise among repeated tests.

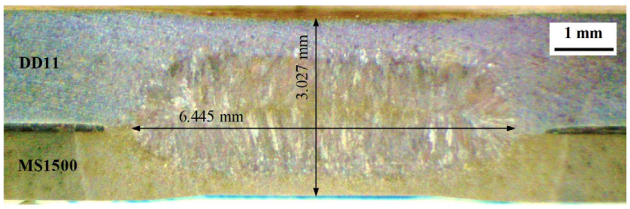

Figure 8: Cross-section view of the welded joint using double-pulse strategy with 8.6 kA and 8.4 kA currents.

The geometric properties of welds performed with different current levels were examined through their cross-sections. The cross-section image of the joint, created using the double-pulse strategy with the highest strength observed at 8.6 kA and 8.4 kA currents, is shown as an example in Fig. 8. The measured nugget diameter values of joints welded with different currents using single-pulse and double-pulse welding strategies are presented in Fig. 9. When these values are analyzed, it is observed that the nugget diameter increases even at the lowest current value when transitioning

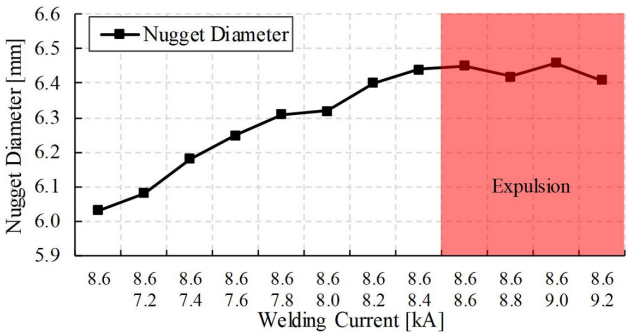

Figure 9: Nugget diameter distribution depending on the welding current.

from the single-pulse to the double-pulse welding strategy. Furthermore, this increase in diameter continues until the double-pulse welding current reaches 8.4 kA. However, when the current value is 8.6 kA or higher, the increase in nugget diameter ceases. This situation is directly associated with expulsion. In the case of expulsion, the liquid metal in the weld area is expelled outside the welding zone. As the molten metal exits the welding zone, the nugget diameter stops increasing. The occurrence of expulsion at currents of 8.6 kA and above is also illustrated in Fig. 7.

The changes in indentation values depending on the welding current and welding strategy are shown in Fig. 10. In the geometry of resistance spot-welded joints, it is desirable to have low indentation values. However, due to the increase in the volume of molten metal during the process, the penetration of the electrodes into the metal increases as a result of the applied force. Especially in the automotive industry, it is expected that the indentation value remains below 10% for aesthetic components. It has been determined that the indentation ratio increases when transitioning from the single-pulse to the double-pulse welding strategy. Additionally, the indentation values show a consistent increase up to a welding current of 8.4 kA. However, at 8.6 kA, a significant upward jump in the indentation value is observed. This is caused by the expulsion and resulting ejection of the molten metal out of the nugget section. As a result, welding electrodes can penetrate the sheet metals more.

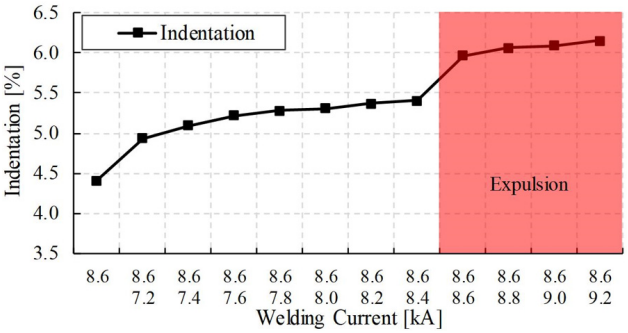

Figure 10: Indentation distribution depending on the welding current.

The hardness distribution along the weld was examined for the specimens produced with the double-pulse welding strategy at the current values yielding the highest strength. The measurement results are shown in Fig. 11. Hardness measurements were conducted at intervals of 0.10 mm. Measurements were taken along the line shown in Fig. 11 starting from the base metal of the DD11 steel, going through the nugget, and ending in the base metal of the MS1500 steel. The most notable observation in the hardness values is a significant increase in hardness in the nugget region of both materials. The initial hardness levels of MS1500 and DD11 steels, which were 365 HV and 135 HV, respectively, increased to about 400 HV within the nugget. Higher hardness in the nugget region of RSW joints compared to the base metal is already reported in former studies about martensitic steels [3, 20]. It is caused by the very high cooling rates in the nugget region of the joint caused by the contact with the cooled copper electrode. As a result, cooling rate may exceed 2000 K/s [3]. Such cooling rates may not be reached in conventional thermos-mechanical processes used in the manufacturing of martensitic steels.

Furthermore, the average hardness in the nugget region of DD11 steel was calculated as 394.9 HV. On the other hand, average hardness in the nugget of MS1500 steel was with 403.2 HV slightly higher. The difference is caused by the higher alloying composition of the MS1500 steel.
Additionally, an increase in hardness was observed in the heat-affected zone (HAZ) of the MS1500 material. No softening was detected in this region. It is caused by the grain refinement of the already existing martensitic structure in the base metal. Conventional martensitic steels are annealed after manufacturing to reduce the brittleness. Such an annealing process also causes a certain amount of grain growth in the microstructure. However, thanks to the rapid cooling after applied RSW process, a significant grain refinement is expected in the heat-affected zone (HAZ) of the joint, which is called as HAZ-hardening in the relevant literature [3].

In contrast to the MS1500 steel, within the DD11 material, the hardness in the HAZ decreased from 400 HV in the nugget to the base metal level of 135 HV over a distance of approximately 1 mm. Due to the low alloying composition of the DD11 steel, martensite formation should be suppressed in that material.

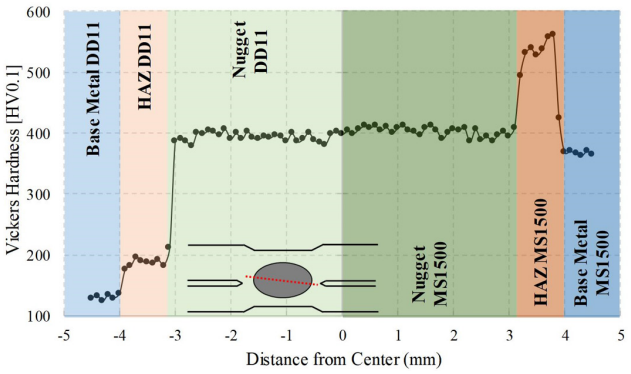

Figure 11: Hardness distribution in welding section.

The hardness behavior of the weld region can be explained through the microstructure analyses shown in Fig. 12. The DD11 steel used in the study has a ferritic-pearlitic microstructure, as shown in Figure 12(a). This ferritic-pearlitic microstructure transformed into a martensitic microstructure due to rapid cooling in the heat-affected zone (HAZ), as shown in Figure 12(b). However, ferrite islands are still visible within this structure. Consequently, the gradual hardness increase observed in Fig. 11 was noted.

As shown in Fig. 12(c), the microstructure of both materials in the nugget is identical. This region contains a martensitic structure, oriented toward the electrodes, which typically forms due to the very rapid cooling seen in resistance spot-welded joints. Fig. 12(d) shows the initial microstructure of the MS1500 material, which consists of a lath martensite structure with well-defined pocket boundaries. Due to the rapid cooling from the austenitic region in the HAZ, this microstructure transformed into fine-grained martensite, as illustrated in Figure 12(e). Accordingly, the hardness increase in the HAZ, shown in Fig 11, was observed.

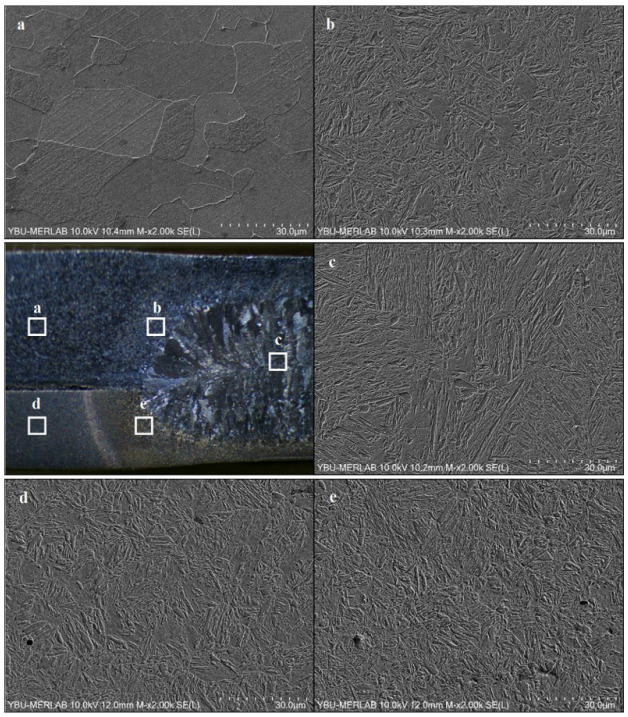

Figure 11: Scanning electron microscopy images of (a) base metal of DD11, (b) heat-affected zone of DD11, (c) nugget section of the joint, (d) base metal of MS1500, and (e) heat-affected zone of MS1500.

CONCLUSION

This study investigated the mechanical and microstructural properties of resistance spot-welded joints produced using single-pulse and double-pulse welding strategies for ultra-high-strength MS1500 steel and hot-rolled DD11 steel. Following conclusions are drawn from the studies:

- It was observed that in the single-pulse welding strategy, expulsion occurred at a welding current of 8.6 kA and above, limiting the mechanical performance of the joints.
- The double-pulse welding strategy could significantly improve the joint strength and failure energy.
- The optimal mechanical properties were achieved with a second welding current of 8.4 kA during the double pulse welding.
- The double-pulse welding strategy with optimum parameters resulted in a tensile-shear strength increase of 11.6% and a fracture energy improvement of 32.2% compared to the single-pulse strategy.
- During double pulse welding, when the second welding current exceeded 8.6 kA, expulsion started to occur and affected joint strength and consistency negatively.
- The double-pulse welding strategy with optimum parameters resulted in a nugget diameter of 6.445 mm which corresponds to an increase of 6.8% compared to single-pulse welding strategy.
- There was a slight increase in the indentation rate when using the double-pulse welding strategy. This rate increased from 4.41% at the single-pulse welding to 5.41% at the optimum double-pulse welding strategy.
- Microstructural analyses on DD11 steel indicated that the transformation of the ferritic-pearlitic structure in the heat-affected zone (HAZ) to martensitic microstructures contributed to the hardness increase.

The findings demonstrate the potential of the double-pulse welding strategy in enhancing the performance of resistance spot-welded joints, especially for applications requiring high strength and minimal deformation. Future studies could explore further optimization of current levels and welding durations to refine the double-pulse strategy for broader industrial applications.

Acknowledgement

The authors wish to thank the Turkish Research Council (TÜBİTAK) for financially supporting the project 5190043.

References

1. Jeswiet J, Geiger M, Engel U, Kleiner M, Schikorra M, Duflou J, Neugebauer R, Bariani P. Bruschi S. Metal forming progress since 2000. CIRP J. Manuf. Sci. Technol. 2008, 11: 2-17. https://doi.org/10.1016/j.cirpj.2008.06.005
2. Kimchi M, Philips DH. Resistance Spot Welding – Fundamentals and Applications for the Automotive Industry. 2nd edition. Switzerland, Springer Nature; 2023.
3. Pouranvari M, Marashi SPH. Critical review of automotive steels spot welding: process, structure and properties, Sci. Technol. Weld. Join. 2013; 18(5):361-403. https://doi.org/10.1179/1362171813Y.0000000120
4. Zhang H, Senkara J. Resistance Welding – Fundamentals and Applications. 2nd edition. Boca Raton: CRC Press; 2011.
5. Chabok A, van der Aa E, De Hosson JTM, Pei YT. Mechanical behavior and failure mechanism of resistance spot welded DP1000 dual phase steel. Mater. Des. 2017; 124:171-182. http://dx.doi.org/10.1016/j.matdes.2017.03.070
6. Noh W, Kim W, Yang X, Kang M, Lee M-G, Chung K. Simple and effective failure analysis of dissimilar resistance spot welded advanced high strength steel sheets. Int. J. Mech. Sci. 2017; 121:76-89. http://dx.doi.org/10.1016/j.ijmecsci.2016.12.006
7. Sivaraj P, Seeman M, Kanagarajan D, Seetharaman R. Influence of welding parameter on mechanical properties and microstructural features of resistance spot welded dual phase steel sheets joint. Mater. Today: Proc. 2020; 22(23):558-562. https://doi.org/10.1016/j.matpr.2019.08.201
8. Jaber HL, Pouranvari M, Salim RK, Hashim FA, Marashi SPH. Peak load and energy absorption of DP600 advanced steel resistance spot welds. Ironmak Steelmak. 2017; 44(9):699-706. https://doi.org/10.1080/03019233.2016.1229880
9. Chabok A, van der Aa E, Basu I, De Hosson JTM, Pei Y. Effect of pulse scheme on the microstructural evolution, residual stress state and mechanical performance of resistance spot welded DP1000-GI steel. Sci. Technol. Weld. Join. 2018; 23(8):649-658. https://doi.org/10.1080/13621718.2018.1452875
10. Pouranvari M, Aghajani H, Ghasemi A. Enhanced mechanical properties of martensitic stainless steels resistance spot welds enabled by in situ rapid tempering. Sci. Technol. Weld. Join. 2020; 25(2):119-126. https://doi.org/10.1080/13621718.2019.1641962
11. Kim JW, Murugan, SP, Yoo, JH, Ashiri R, Park YD. Enhancing nugget size and weldable current range of ultra-high-strength steel using multi-pulse resistance spot welding. Sci. Technol. Weld. Join. 2019; 25(3):235-242. https://doi.org/10.1080/13621718.2019.1680483

12. Soomro IA, Pedapati SR, Awang M. Optimization of postweld tempering pulse parameters for maximum load bearing and failure energy absorption in dual phase (DP590) steel resistance spot welds. Mater. Sci. Eng. A. 2021; 803:140713. https://doi.org/10.1016/j.msea.2020.140713
13. Liu XD, Xu YB, Misra RDK, Peng F, Wang Y, Du YB. Mechanical properties in double pulse resistance spot welding of Q&P 980 steel. J. Mater. Process. Technol. 2019; 263: 186-197. https://doi.org/10.1016/j.jmatprotec.2018.08.018
14. Mousavi Anijdan SH, Sabzi M, Ghobeiti-Hasab M, Roshan-Ghiyas A. Optimization of spot welding process parameters in dissimilar joint of dual phase steel DP600 and AISI 304 stainless steel to achieve the highest level of shear-tensile strength. Mater. Sci. Eng. A. 2018; 726:120-125. https://doi.org/10.1016/j.msea.2018.04.072
15. Yuan X, Li C, Chen J, Li X, Liang X, Pan X. Resistance spot welding of dissimilar DP600 and DC54D steels. J. Mater. Process. Technol. 2017; 239:31-41. http://dx.doi.org/10.1016/j.jmatprotec.2016.08.012
16. Zhang H, Qiu X, Xing F, Bai J, Chen J. Failure analysis of dissimilar thickness resistance spot welded joints in dual-phase steels during tensile shear test. Mater. Des. 2014; 55:366-372. http://dx.doi.org/10.1016/j.matdes.2013.09.040
17. Onar V. Mechanical and Microstructural Characterizations of Resistance Spot Welded Dissimilar TWIP/304L Stainless Steel. Trans. Indian Inst. Met. 2022; 75(7):1731-1739. https://doi.org/10.1007/s12666-021-02446-9
18. Özen F, Onar V, Bulca M, Aslanlar S. Resistance spot weldability of Fe-15.4Mn-2.1Al-1.2C twinning induced plasticity steel. Materialwiss. Werkstofftech. 2023; 54:857–870. https://doi.org/10.1002/mawe.202200241
19. Özen F. Mechanical and microstructural characterization of resistance spot welded dissimilar TWIP1000/TRIP800 joints. Mater. Test. 2024; 66(1):9-21.
20. Özen F, Aslanlar S. Mechanical and microstructural evaluation of resistance spot welded dissimilar TWIP/martensitic steel joints. J. Adv. Manuf. Technol. 2021; 113:3473-3489. https://doi.org/10.1007/s00170-021-06848-3